

# X-rays and Fluctuating X-Winds from Protostars

Frank H. Shu,\* Hsien Shang, Alfred E. Glassgold, Typhoon Lee

Protostars emit more x-rays, hard and soft, than young sunlike stars in more advanced stages of formation. The x-ray emission becomes harder and stronger during flares. The excess x-rays may arise as a result of the time-dependent interaction of an accretion disk with the magnetosphere of the central star. Flares produced by such fluctuations have important implications for the x-wind model of protostellar jets, for the flash-heating of the chondrules found in chondritic meteorites, and for the production of short-lived radioactivities through the bombardment of primitive rocks by solar cosmic rays.

Copious x-ray emission provides one of the strongest pieces of evidence for enhanced magnetic activity on the surfaces of young sunlike stars (1). Much of the early information derived from measurements at relatively soft energies ( $\sim 0.4$  to 4 keV) by the focusing x-ray telescope borne into space on the Einstein satellite (2). The majority of the young stellar objects (YSOs) observed by the Einstein satellite belong to the category of optically revealed sources without circumstellar disks known as weak-lined T Tauri stars (WTTs). WTTs and their counterparts with nebular disks known as classical T Tauri stars (CTTs) are believed to have ages of one to a few million years (3). They represent a later phase of young star evolution than embedded protostars, which undergo not only active disk accretion but also infall from their surrounding molecular cloud cores (4). The surrounding envelope absorbs much of the soft x-rays from the central protostar, making embedded protostars difficult to detect by the Einstein satellite.

The Einstein measurements gave rise to the analogy of T Tauri stars (TTSs) as objects with surface magnetic activity much like that of the sun at present, except magnified manyfold. TTSs have typical soft x-ray luminosities of  $\sim 3 \times 10^{29}$  erg s $^{-1}$  (5), and the flares that arise in them can be  $\sim 10^6$  times as strong as the sun (6). In the sun, soft x-ray flares originate in hot coronal gas (temperature  $T \sim 10^7$  K) trapped in loops of intense magnetic field (7). Models of the soft x-ray flares on TTSs assume

similar temperatures, but larger loop sizes ( $\sim 10^{11}$  cm high), and imply plasma densities of  $\sim 10^{10}$  cm $^{-3}$  and magnetic field strengths of  $\sim 10^3$  G at the base of the loops that are not very different from those of the modern sun (1).

Recent observations of YSOs at hard x-ray energies (0.4 to 12 keV) by the ASCA satellite and to deeper sensitivity levels at soft x-ray energies (0.1 to 2.4 keV) by the Roentgen x-ray satellite (ROSAT) have motivated a reevaluation. Except for XZ Tau (8), a single source, CTTs generally emit fewer x-rays than WTTs (9), probably because interactions with circumstellar disks slow down the rotation of CTTs with respect to WTTs (10). On the other hand, embedded protostars appear to be more powerful and harder x-ray emitters than either WTTs or CTTs (11). The x-ray spectra of YSOs harden during x-ray flares. The soft x-rays may come from a mechanism of heating stellar coronas common to all stars with surface magnetic activity whether or not they have surrounding accretion disks. The hard x-rays probably arise from fast particle acceleration and deceleration events.

The mean luminosity in hard x-rays of several embedded protostellar sources discovered by the ASCA satellite in the nearby dark cloud R CrA is  $L_x^{\text{hard}} = 3 \times 10^{30}$  erg s $^{-1}$  (11). A recent sampling of embedded protostars indicated an average luminosity in total x-rays, corrected for the effects of envelope absorption and finite ROSAT bandwidth,  $L_x^{\text{tot}} \geq 10^{31}$  erg s $^{-1}$  (12). Of the latter value, we assume that an amount  $10^{29}$  to  $10^{30}$  erg s $^{-1}$  can be associated with “normal” coronal plasma at  $T \sim 10^7$  K similar to that observed in WTTs. The rest we attribute to heating by fast particles generated in big and small flares.

**Fast particles associated with x-ray flares.** Fast particles in the sun originate in two types of flares (13) through the release of the energy stored in stressed

magnetic fields (14). Impulsive flares, lasting typically only tens of minutes, are electron and  $^3\text{He}$  rich and probably arise low in the solar corona in reconnection events involving closed magnetic field lines. The fast electrons generated by the flare stream along the field lines to their foot points in the solar photosphere, releasing visible and hard x-ray photons when they strike the surface of the sun. The accompanying fast protons and ions produce gamma rays in their interactions with the solar atmosphere.

On the sun, there are also proton-rich events that release large numbers of cosmic ray ions without producing many photons either in visible light or in x-rays (15, 16). Rarer by a factor of  $\sim 10$  but lasting from hours to days when they occur, gradual flares arise high in the solar corona, perhaps in magnetic field configurations called flare loops or helmet streamers [see figure 5 in (14)]. Magnetic energy released in the helmet streamer (coming before reconnection of oppositely directed field lines) drives violent outward motions in the surrounding plasma, leading to coronal mass ejections (CMEs). Magnetohydrodynamic shock waves associated with CMEs then accelerate copious numbers of solar energetic particles, initiating, in the case of the solar system, geomagnetic storms when they interact downstream with Earth’s magnetosphere.

**Enhanced disk-magnetosphere interactions in protostars.** The total photon luminosity of an embedded protostar is comparable to that of a CTT [see figure 6 in (17)]. Why then does the former emit so much more energy in hard and soft x-rays (10)? Alternatively, why does the former accelerate so many more fast particles? Because one big difference between an embedded protostar and a CTT is the rate at which disk accretion occurs (18), the underlying cause may involve the enhanced interaction between the stellar magnetosphere and the surrounding accretion disk, similar to phenomena that astronomers see in binary x-ray sources and cataclysmic variables (19).

To develop this speculation into a useful tool for the analysis of YSOs, we need a concrete model of the interaction. Here, we adopt the x-wind model (20), which has been described previously as the underlying mechanism for the production of calcium-aluminum-rich inclusions (CAIs) and chondrules in chondritic meteorites (21). In fact, x-ray astronomers have long held the conviction that x-rays provide the crucial link that might unify seemingly disparate aspects of the rich phenomenology that involves YSOs: magnetic activity, protostellar winds and jets, and extinct radio-

F. Shu is at the Astronomy Department, University of California, Berkeley, CA 94720-3411, USA, and the Institute of Astronomy and Astrophysics, Academia Sinica, Taipei 115, Taiwan. H. Shang is in the Astronomy Department, University of California, Berkeley, CA 94720-3411, USA. A. E. Glassgold is in the Physics Department, New York University, New York, NY 10003, USA. T. Lee is at the Institute of Earth Science and the Institute of Astronomy and Astrophysics, Academia Sinica, Taipei 115, Taiwan.

\*To whom correspondence should be addressed.

activities in meteorites (1, 22).

**The x-wind model.** In the x-wind model (see Fig. 1), the interaction of mass accretion at a rate  $\dot{M}_D$  through a disk with the magnetosphere of a protostar of mass  $M_*$  and magnetic dipole moment  $\mu_*$  truncates the gas disk at an inner edge at a radius  $R_x$  larger than the stellar radius  $R_*$ . The disk accretion divides at  $R_x$  into an x-wind outflow with mass loss rate  $\dot{M}_w = f\dot{M}_D$  and a funnel inflow onto the star at rate  $\dot{M}_* = (1 - f)\dot{M}_D$ , where the fraction  $f$  is obtained by considerations of angular-momentum balance in the steady state. This balance regulates the spin rate of the central star  $\Omega_*$  to the Keplerian angular velocity  $\Omega_x$  of the inner edge of the gaseous disk with which the star shares common field lines.

The equilibrium state is characterized by  $\Omega_* = \Omega_x$ , because if corotation did not hold, the subsequent generation of magnetic torques would tend to reduce the discrepancy between  $\Omega_*$  and  $\Omega_x$ . To understand, imagine that  $\Omega_*$  is larger than  $\Omega_x$ . When the star turns faster than the inner edge of the disk, the field lines that attach to both would continuously wrap into ever tighter trailing spirals. Trailing spiral patterns of magnetic field lines transfer angular momentum outward (23), with the field lines adjacent to the star tugging it backward in the sense of rotation. This tug decreases the star's angular rate of rotation  $\Omega_*$  to more nearly equal the rate  $\Omega_x$ . Conversely, if  $\Omega_*$  is smaller than  $\Omega_x$ , the field lines attached to both would continuously wrap into ever tighter leading spirals, transferring angular momentum inward and increasing  $\Omega_*$  again to more nearly equal the rate  $\Omega_x$ . In true steady state,  $\Omega_*$  exactly equals  $\Omega_x$ , with the funnel-flow field lines acquiring just enough of a trailing spiral pattern (but without continuously wrapping up) so that the excess of material angular momentum brought toward the star by the inflowing gas is transferred outward by magnetic torques

to the foot points of the magnetic field in the disk (24).

In reality, two surfaces of null poloidal field lines are required to mediate the geometry of dipole-like field lines of the star with those opened by an x-wind and those trapped by a funnel inflow emanating from the x-region. Labeled as "helmet streamer" and "reconnection ring" in Fig. 1, these magnetic null surfaces begin or end on "Y points" [called "kink points" in (24)]. Across each null surface, the poloidal magnetic field suffers a sharp reversal of direction. By Ampère's law, large electric currents must flow out of the plane shown in Fig. 1 along the null surfaces. In the presence of nonzero electrical resistivity, dissipation of these currents would lead to reconnection of the oppositely directed field lines (25). Reconnection would reduce the total amount of trapped magnetic flux in the x-region, which would modify the numerical value of the coefficient of the equation relating  $R_x$  to  $M_*$ ,  $\mu_*$ , and  $\dot{M}_D$  (24).

When  $R_x$  changes, the Keplerian angular speed of the foot point of magnetic field lines in the x-region will also vary. However, the star has too much inertia for its angular velocity  $\Omega_*$  to alter appreciably on the time scale of magnetic reconnection at the null surfaces of the magnetosphere. With  $\Omega_*$  different from  $\Omega_x$ , field lines attached to both the star and the disk will be stretched and amplified by the resultant shear. The increased magnetic pressure of the growing toroidal field will cause the poloidal fields to bulge outward, which would tend to insert more poloidal field into the fan of field lines emanating from the x-region. The upward-rising dipole-like poloidal fields would ultimately have to be replaced by dynamo action inside the star. This dynamo action would be enhanced because, in addition to any stellar differential rotation,  $\Omega_*$  differs from  $\Omega_x$ . In principle, a secular balance might be reached,

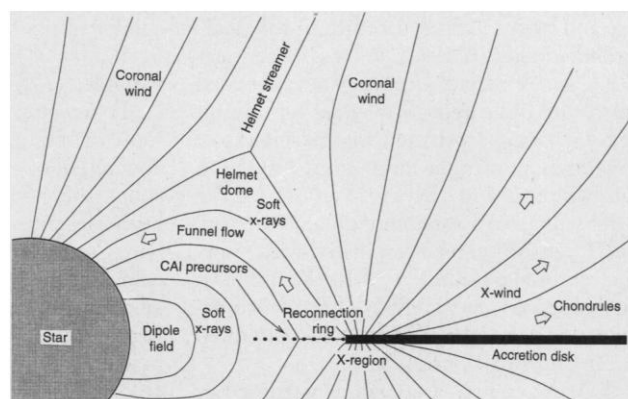
with the dynamo-generated poloidal fields being inserted steadily to offset a steady rate of field dissipation at the null surfaces. In practice, observation of the sun teaches us otherwise. The dissipation and reconnection of magnetic field lines and their resupply are likely to occur not steadily, but sporadically, involving violent flares followed by more gradual recoveries to the preflare magnetic configuration.

**The astronomical evidence for fluctuating x-winds.** The spectral lines that diagnose for gas above the atmospheres of TTSs vary from night to night of observation (26). Time-series analyses of two such systems revealed a periodicity in diagnostic hydrogen lines for inflow and outflow, with the repetition time equal to the rotation period of the star (27). If the inner disk edge is indeed the source for the hydrogen gas in the funnel flow and x-wind (but driven perhaps by a tilted rather than an aligned magnetic dipole), then these two systems do satisfy the equilibrium condition  $\Omega_x = \Omega_*$ . However, the majority of cases examined show no obvious periodicities (28), indicating that either  $\Omega_* \neq \Omega_x$  as a general instantaneous condition or the stellar magnetic dipole is usually aligned too well with the spin axis of the disk to give noticeable azimuthal asymmetries that would translate by rotation to a temporal periodicity.

Time variations considerably longer than days are also known for YSO flows. The spacing and fast motions of emission knots (or Herbig-Haro objects) emanating from YSOs (29) have inspired models of pulsed protostellar jets (30), suggesting that the mass outflows from the central regions vary on time scales of years to hundreds of years (perhaps associated with dynamo cycles like those governing the 11-year sunspot cycle). On even longer time scales (thousands of years), systems in the embedded phase of evolution undergo dramatic FU Orionis outbursts (31), which are currently modeled as large increases in  $\dot{M}_D$  for decades to hundreds of years, followed by a long period of relative quiescence before the system undergoes a new cycle of enhanced  $\dot{M}_D$ .

We conclude that even if  $\Omega_*$  equals  $\Omega_x$  as a long-term average,  $\Omega_*$  will not generally equal  $\Omega_x$  instantaneously. This causes no problems for the x-wind outflow (20), because this outflow occurs on open field lines disconnected from the star, and the only requirement for the operation of the magnetocentrifugal drive is that the foot point of the field in the disk rotates at the local Keplerian speed  $\Omega_x$ . However, the condition  $\Omega_* \neq \Omega_x$  does create a problem for steady-state funnel flow. The result is enhanced x-ray flaring, particularly in hard x-rays.

**Fig. 1.** Schematic drawing of the magnetic field geometry and gas flow in the x-wind model for the production of CAIs and chondrules. While chondrules are being launched from the x-region, cosmic-ray irradiation of CAI precursors occurs by impulsive flares in the reconnection ring, where the distorted dipole field lines make an excursion to the x-region as a part of the magnetic flux trapped there. The figure indicates that thermally driven coronal winds from the star and the disk may help the magnetocentrifugally driven x-wind to open field lines surrounding the helmet streamer, but this aspect of the configuration is not essential to our model.



**Implications for CAI and chondrule formation.** We now consider the consequence of a fluctuating x-wind for the production of CAIs and chondrules by the radiative heating and melting of dustballs brought by disk accretion to the inner edge of the disk (21). The reconnection ring lies below the funnel flow and will therefore temporarily contain millimeter- to centimeter-sized solids that drop out as molten spheres from the funnel gas on the way from the x-region to the star. Solids can also drift into the reconnection ring from the x-region by the drag exerted by more slowly orbiting gas (32). In other words, the inner edge of the dust disk will generally lie at a smaller radius than the inner edge of the gas disk. This conclusion agrees with efforts to model the near-infrared spectral energy distribution of CTTs, which often require optically thick dust disks to extend inward to the dust evaporation point for CAI-like material (33). If these solids were left to themselves, they would slowly spiral inward through the equatorial plane and accrete (as vapor) onto the sun, much as the icy particulates composing Saturn's ring gradually migrate toward that planet through a variety of angular-momentum transport processes. Before this happens, however, an inward fluctuation of the location of the base of the x-wind might scour this region free of its solids.

To fix ideas, we consider specific numerical examples constructed to mimic the effects of magnetic cycles in the two fiducial cases considered in (21). Over the course of a decade, say, the stellar magnetic moment  $\mu_*$  varies by a factor 2 or 3 about the mean. The formulas given in (21) plus the values cited or calculated there for  $M_*$ ,  $R_*$ ,  $L_*$ ,  $\dot{M}_D$ ,  $\dot{M}_w$ , and  $\alpha \equiv 3C_D \dot{M}_w / 16\pi \Omega_x R_x^2 \rho_c R_c$ , where  $L_*$  is the stellar luminosity,  $\dot{C}_D$  is the drag coefficient,  $\rho_c$  is the internal density of a CAI or chondrule precursor, and  $R_c$  is the radius of a CAI or chondrule precursor, lead to the results listed in Tables 1 and 2.

Temporal variations of 40 or 50 km s<sup>-1</sup> in the wind's terminal velocity  $\bar{v}_w$  about the average value should give reasonable shock speeds, temperatures, and ionization fractions for pulsed models of magnetized stellar jets. In the high magnetic state of the embedded protostar in Table 1, the base temperature  $T_x$  is 750 K, which is not quite low enough (680 K) to allow the precursor rocks to retain FeS (34). Chondrules produced during the high magnetic state of the revealed CTTs in Table 2, when  $T_x = 500$  K, do better. When launched in the high state of the fiducial embedded source, rocks acquire and maintain peak temperatures  $\bar{T}_{peak}$  near 1300 K for a few days. This allows the partial retention of sodium and potassium in the rocks as long as the oxygen

fugacity in the x-wind is sufficiently high [see the discussion in (21)]. Chondrules launched in the x-wind during the high state of the fiducial-revealed source do not even require the benefits of high-oxygen fugacity to retain their sodium because  $\bar{T}_{peak}$  reaches only 950 K in this case. The typical diameters  $2R_c = 3.0$  and 0.14 mm of the rocks that return to the disk are comparable to the chondrules found in carbonaceous and ordinary chondrites, respectively. Unfortunately, in both cases, the  $\bar{T}_{peak}$  values reached in the x-wind are insufficient to melt magnesium-iron silicates and hence to produce the textures and droplet shapes of chondrules.

Flares exploding near the x-region before the launch of the chondrules may provide a solution to the above difficulty. The peak x-ray luminosity reached in the most powerful flares can rival the photon luminosity of the system at all other wavelengths (12). The extra radiative heating provided by such flares can cause the base value of  $T_x$  to double or triple while the protochondrule lies near the x-region. The large effect arises because the x-ray energy is released either close to the rocks (when the flare goes off in the reconnection ring) or above them in a geometry that does not involve very oblique rays (when the flare goes off in the helmet streamer). If the doubling or tripling of  $T_x$  causes the protochondrule to vaporize, no harm is done, because the constituent atoms will simply recondense somewhere else as a dustball (or as a rim onto a preexisting proto-CAI) once the flare has subsided. On the other hand, if the doubling or tripling of  $T_x$  happens to be in the range appropriate to melting protochondrules, then the body stays molten

only for the period of time (tens of minutes for an impulsive flare) that the flare intensity is near its maximum. Such conditions are perfect for producing the observed chondrule textures, while they still allow some chondrules to retain their moderate volatiles (35).

In the low magnetic state, when the inner edge of the gas disk pushes closer to the central star, the  $T_x$  values in the embedded and revealed cases are 1600 and 1100 K, respectively, which are high enough to drive out most of the FeS, Na, and K, especially if the precursor rocks reside for decades at such points before the x-wind scours out the region. When launched, the rocks acquire and maintain  $\bar{T}_{peak}$  values near 2200 and 1600 K for days, which will evaporate most of the magnesium-iron silicates. Then many difficulties disappear (36), leaving primarily a refractory residue of molten or partially molten calcium-aluminum oxides and silicates. The typical sizes  $2R_c$  of 4.9 and 0.22 mm for the rocks that return to the asteroid belt are characteristic of CAIs found in carbonaceous chondrites and ordinary chondrites, respectively. Larger specimens must be produced during fluctuations that have higher values of  $\dot{M}_w$  than assumed for the present calculations.

The melting of protochondrules and the deposition of rims onto proto-CAIs may occur many times before these bodies are ever launched by an encroaching x-wind. The multiplicity of large flare events removes the difficulty encountered in (21) of explaining CAIs with very thick fine-grained rims. In particular, CAIs that are almost entirely composed of successive layers of rims no longer pose a problem for the

**Table 1.** Fluctuating x-wind model in embedded stage.

Quantity	High state	Average state	Low state
$\mu_*$ (G cm <sup>3</sup> )	$6 \times 10^{37}$	$2 \times 10^{37}$	$1 \times 10^{37}$
$R_x$ (cm)	$1.5 \times 10^{12}$	$8.4 \times 10^{11}$	$5.5 \times 10^{11}$
$\Omega_x$ (s <sup>-1</sup> )	$4.4 \times 10^{-6}$	$1.1 \times 10^{-6}$	$2.0 \times 10^{-6}$
$\bar{v}_w$ (km s <sup>-1</sup> )	140	190	230
$T_x$ (K)	750	1200	1600
$\bar{T}_{peak}$ (K)	1300	1800	2200
$2R_c$ (mm)	3.0	3.8	4.9

**Table 2.** Fluctuating x-wind model in revealed stage.

Quantity	High state	Average state	Low state
$\mu_*$ (G cm <sup>3</sup> )	$3 \times 10^{37}$	$1 \times 10^{37}$	$0.5 \times 10^{37}$
$R_x$ (cm)	$2.1 \times 10^{12}$	$1.1 \times 10^{12}$	$7.7 \times 10^{11}$
$\Omega_x$ (s <sup>-1</sup> )	$3.3 \times 10^{-6}$	$8.7 \times 10^{-6}$	$1.5 \times 10^{-5}$
$\bar{v}_w$ (km s <sup>-1</sup> )	150	200	240
$T_x$ (K)	500	800	1100
$\bar{T}_{peak}$ (K)	950	1300	1600
$2R_c$ (mm)	0.14	0.19	0.22

x-wind model. Indeed, with thick mantles likely for proto-CAIs, the evaporation of less refractory material in the x-wind probably removes more rim material from CAIs than is added by in-flight condensation. Moreover, because the temperature swings in the reconnection ring are nonmonotonic, successive layers that survive need not be arranged according to a strict condensation sequence.

Intermediate magnetic states allow for refractory objects that neither melt nor vaporize when exposed to flares or when subsequently launched by the x-wind. Such objects may retain shapes that resemble fluffy aggregates. If these fluffy aggregates are sufficiently large and dense, they will not couple perfectly to the x-wind by gas drag, and they can reenter the disk after traveling to planetary distances. Is this the origin of the amoeboid olivine inclusions found in chondritic meteorites? Would the carrying of the smaller or less dense counterparts of these bodies to interstellar space by the x-wind explain the loss of such refractories in ordinary chondrites [see figure 7.3.6 of (37) and the discussion on page 1550 of (21)]?

Over a complete magnetic cycle (decades), the examples given in Table 1 and 2 can produce both CAIs and chondrules. If the CAIs and chondrules thrown to the main asteroid belt accrete there onto bodies larger than  $\sim 10^4$  m, we need not worry that CAIs and chondrules have inward radial drift time scales of only  $\sim 10^4$  years (32). For accretion times onto parent bodies shorter than the YSO evolution time of about a million years, the size differences in CAIs and chondrules produced during the embedded and revealed stages can be maintained in the resultant meteorites. We address the question of the relative frequencies with which CAIs and chondrules are found in carbonaceous and ordinary chondrites after we first consider the gross energetics of magnetic energy release in the x-wind model.

**Rate of magnetic energy release.** When  $\Omega_* \neq \Omega_x$ , dimensional analysis of the funnel-flow configuration gives the rate of increase of magnetic energy  $E_{\text{mag}}$  as

$$\frac{dE_{\text{mag}}}{dt} = \eta |\Omega_* - \Omega_x| \frac{\mu_*^2}{R_x^3}, \quad (1)$$

where  $\eta$  is a dimensionless form factor that incorporates the details of the specific field geometry. In the x-wind model of Fig. 1, where only a third of the field lines trapped by the x-region are tied to the star, giving rise to funnel flows that end on hot spots occupying several percent of the surface area of the star (24), we expect  $\eta < 1$ . Numerical simulations of solar flares suggest

that the disruption of helmet streamers triggers CMEs on the sun when the accumulated shear has increased the field energy to a point where ejection of magnetized plasmoids opens the field lines under the helmet dome [see figures 1 and 2 in (38) and also the simulations in (39)]. For the geometry applicable to YSO funnel flow, the analogous process in the reconnection ring will also sporadically inject fresh poloidal fields to be trapped by the x-region, offsetting later reconnection losses.

Applied to the examples of Tables 1 and 2, we suppose that the star has an angular velocity equal to  $\Omega_x$  of the average states,  $\Omega_* = 1.1 \times 10^{-5}$  and  $8.7 \times 10^{-6} \text{ s}^{-1}$ . The scale  $|\Omega_* - \Omega_x| \mu_*^2 / R_x^3$  for disk-augmented magnetic energy release is therefore  $7.0 \times 10^{33}$  and  $5.2 \times 10^{32} \text{ erg s}^{-1}$  during the high states, and it is  $5.4 \times 10^{33}$  and  $3.4 \times 10^{32} \text{ erg s}^{-1}$  in the low states. These scalings suggest, for both high and low states, that the model in Table 1 is  $\sim 15$  times more powerful an x-ray emitter than the model in Table 2, with most observed CTTSs probably in a more advanced stage of evolution than in the fiducial example in Table 2.

The above conclusions are insensitive to the specific numbers used in the models. We obtain the x-ray luminosity from  $L_x^{\text{tot}} = \epsilon_x dE_{\text{mag}}/dt$ , where  $\epsilon_x$  is the efficiency for generating x-rays and is  $< 1$  because some of the magnetic energy release goes into the kinetic energy of CMEs, accelerating fast particles, and other wave bands. If we now write  $|\Omega_* - \Omega_x| \equiv S\Omega_x$ , where  $S$  is a number of order unity, and if we eliminate  $\mu_*$  from Eq. 1 by using equation 1 of (21), we get

$$L_x^{\text{tot}} = \epsilon_x \eta S \Phi_{\text{dx}}^2 \frac{GM_* M_{\text{D}}}{R_x}, \quad (2)$$

where  $\Phi_{\text{dx}} = 1.15$  in the model preferred by (24) and  $G$  is the universal gravitational constant. Thus, with everything else relatively equal, the release of magnetic energy is proportional to the disk-accretion energy scale  $GM_* M_{\text{D}} / R_x$ , which is larger in earlier stages than later ones. Because  $L_x^{\text{tot}}$  measured observationally is much lower than the scale  $GM_* M_{\text{D}} / R_x$ , the product  $\epsilon_x \eta S$  must be  $\ll 1$ .

**Soft x-rays, plasma drag, and survival time of proto-CAIs.** Coronal plasma at  $\sim 10^7$  K can be trapped by closed loops of magnetic field only if the pressure of the hydrogen plasma,  $\sim 2n_e kT$ , where  $n_e$  is the electron density and  $k$  is Boltzmann's constant, is less than the magnetic pressure,  $B^2/8\pi$ , at the weakest point of the loop. For the average state in the fiducial model of Table 1, the magnetic fields below the Y points in Fig. 1 measure  $\lesssim 10$  G. With the

other cited values, our constraint becomes  $n_e \lesssim B^2/16\pi kT \lesssim 1 \times 10^9 \text{ cm}^{-3}$ . From thermal bremsstrahlung theory, we can calculate that a hydrogen plasma of  $n_e \lesssim 10^9 \text{ cm}^{-3}$  and  $T \sim 10^7$  K, confined to a volume  $\sim R_x^3 \sim 10^{36} \text{ cm}^3$ , will radiate a luminosity,  $L_x \lesssim 10^{30} \text{ erg s}^{-1}$  (5), consistent with the assumption made at the outset that most of the total x-ray luminosity inferred from ROSAT observations for protostars is associated with heating by fast particles enhanced by strong disk-magnetosphere interactions.

The plasma tied to field lines attached to the star corotate with the star, but rocks in the reconnection ring rotate at a local Keplerian angular speed  $\Omega > \Omega_*$  on average. The slip occurs at relative velocity  $\Delta v \equiv (\Omega - \Omega_*)R$ , which is typically less than the thermal velocity  $v_T$  of the coronal hydrogen ions. The resultant drag has an associated spiral-in time of  $\sim \rho_c R_c v / \rho_g v_T \Delta v$ , where  $\rho_c \approx 3 \text{ g cm}^{-3}$  and  $\rho_g$  and  $v = R\Omega$  are the mass density and Keplerian speed, respectively, of the ambient gas. With  $\rho_g \sim 5 \times 10^{-16} \text{ g cm}^{-3}$  ( $n_e \sim 3 \times 10^8 \text{ cm}^{-3}$ ),  $v_T \sim 3 \times 10^7 \text{ cm s}^{-1}$  ( $T \sim 10^7$  K), and  $v \sim 3\Delta v \sim 1 \times 10^7 \text{ cm s}^{-1}$  for  $R$  equal to 80% of the corotation radius, the spiral-in time is  $\sim 10$  years for a proto-CAI of diameter  $2R_c \sim 1$  cm, but it is only  $\sim 1$  year for one of diameter  $2R_c \sim 1$  mm. Thus, if normal CAIs are produced from precursor rocks deep inside the reconnection ring during the average state, fluctuations in the x-wind on a time scale  $\Delta t \sim 10$  years have a reasonable chance of retrieving the CAIs when they have the centimeter sizes that characterize the larger CAIs of carbonaceous chondrites. However, under the same conditions, the fluctuating x-wind would find it difficult to retrieve CAIs of the millimeter and smaller sizes that occur in ordinary chondrites. Perhaps this yields another reason, in addition to those given in (21), why CAIs are abundant in carbonaceous chondrites and rare in ordinary ones.

**Extinct radioactivities in meteorites.** Fluctuating x-winds also have the potential of reviving a discarded explanation for the extinct radioactivities found in meteorites (40): bombardment of rocks by cosmic rays from the young sun (41, 42). This possibility has conventionally fundered on the fact that a proton plus alpha fluence sufficient to synthesize  $^{41}\text{Ca}$ , and  $^{53}\text{Mn}$  at meteoritic levels fails by one to two orders of magnitude to produce enough  $^{26}\text{Al}$ . However, impulsive flares arising from reconnection events in the reconnection ring, where CAI precursors lie before they are launched by an inwardly encroaching x-wind, accelerate numerous  $^3\text{He}$  nuclei to mega-electron volts per nucleon and high-

er energies. Such particles, competitive in numbers to protons and alphas in impulsive flares (16), can yield  $^{26}\text{Al}$  by the exothermic reaction  $^{24}\text{Mg}(^3\text{He}, p)^{26}\text{Al}$ . Unfortunately, a corresponding reaction,  $^{40}\text{Ca}(^3\text{He}, 2p)^{41}\text{Ca}$ , overproduces  $^{41}\text{Ca}$  by about two orders of magnitude if the  $^3\text{He}$  fluence suffices to give  $^{26}\text{Al}$  at the required meteoritic levels (42). The overproduction of  $^{41}\text{Ca}$  relative to  $^{26}\text{Al}$  can be avoided if proto-CAIs have thick mantles of less refractory rock surrounding more refractory cores, as described in the section "Implications for CAI and chondrule formation." Then,  $^3\text{He}$  nuclei of about a few mega-electron volts per nucleon are stopped in an outer rock layer of thickness  $\sim 60\ \mu\text{m}$  after they have had a chance to interact with the target atoms  $^{24}\text{Mg}$  for producing  $^{26}\text{Al}$  but before they have penetrated to the core to interact with the target atoms  $^{40}\text{Ca}$  for producing  $^{41}\text{Ca}$ . Upon launch in the x-wind, the  $^{26}\text{Al}$  atoms will diffuse to the calcium-aluminum-rich core, whereas most of the magnesium-rich mantle evaporates away, leaving the thin rims found on normal CAIs.

We present elsewhere a full exposition of this topic (42). For the present, we merely note that if  $^{26}\text{Al}$  is produced within the solar system at different levels in CAIs and chondrules rather than seeded at a single uniform value from outside (36), then many difficulties disappear with having to form CAIs a few million years earlier than chondrules, and having to store the former in the nebular disk while waiting for the latter to emerge (32). Thus, the extension of the theory of x-winds to include the notion of fluctuations opens for quantitative investigation, within a single framework, three subjects inaccessible to the steady-state model: the enhanced generation of x-rays in YSOs, the flare-heating of chondrules, and the solar cosmic-ray synthesis of short-lived radioactivities in meteorites.

## REFERENCES AND NOTES

1. T. Montmerle, E. D. Feigelson, J. Bouvier, P. André, in *Protostars and Planets III*, E. H. Levy and J. I. Lunine, Eds. (Univ. of Arizona Press, Tucson, AZ, 1993), pp. 689–720.
2. F. W. Walter, *Astrophys. J.* **306**, 573 (1986); E. D. Feigelson, M. S. Giampapa, F. J. Vrba, in *The Sun in Time*, C. P. Sonnett, M. S. Giampapa, M. S. Matthews, Eds. (Univ. of Arizona Press, Tucson, AZ, 1990), pp. 658–681.
3. C. Bertout, *Annu. Rev. Astron. Astrophys.* **27**, 351 (1989).
4. F. H. Shu, F. C. Adams, S. Lizano, *ibid.* **25**, 23 (1987).
5. E. D. Feigelson and W. M. DeCampli [*Astrophys. J.* **243**, L89 (1981)] cited an average soft x-ray luminosity for TTSs of  $10^{30}\ \text{erg s}^{-1}$ , but this overestimate is now known to have arisen as a result of the sensitivity limit of the Einstein Observatory. More recent analyses of data from ROSAT by E. D. Feigelson *et al.* [*ibid.* **416**, 623 (1993)] and S. Casanova, T. Montmerle, E. D. Feigelson, and P. André [*ibid.* **439**, 752 (1995)] have indicated a more typical value of  $3 \times 10^{29}\ \text{erg s}^{-1}$ .
6. T. Montmerle, L. Koch-Miramond, E. Falgarone, J. E. Grindlay, *Astrophys. J.* **269**, 182 (1983).
7. H. Hudson, in *Proceedings of Kofu Symposium*, Nobeyama Radio Observatory (NRO), Kofu, Japan, 6 to 10 September 1993, S. Enome and T. Hirayama, Eds. (NRO Report No. 360, NRO, Nagano, Japan, 1994), pp. 1–10; L. Acton *et al.*, *Publ. Astron. Soc. Jpn.* **44**, L71 (1992); Y. Uchida *et al.*, *ibid.* **44**, L155 (1992); B. Haisch, K. T. Strong, M. Rodonò, *Annu. Rev. Astron. Astrophys.* **29**, 275 (1991).
8. L. Carkner, E. D. Feigelson, K. Koyama, T. Montmerle, I. N. Reid, *Astrophys. J.* **464**, 286 (1996).
9. E. D. Feigelson, J. M. Jackson, R. D. Mathieu, P. C. Myers, F. M. Walter, *Astron. J.* **94**, 1251 (1987).
10. R. Neuhäuser, *Science* **276**, 1363 (1997).
11. K. Koyama, S. Ueno, N. Kobayashi, E. D. Feigelson, *Publ. Astron. Soc. Jpn.* **48**, L87 (1996); R. Neuhäuser and T. Preibisch, *Astron. Astrophys.* **322**, L37 (1997).
12. For protostars in R CrA, Rho Oph, and NGC 1333, the observed x-ray luminosities in the ROSAT energy band (0.4 to 2.4 keV) are  $10^{30}$  to  $10^{31}\ \text{erg s}^{-1}$  after corrections for envelope extinction, which are considerable (10). N. Grosso *et al.* [*Nature* **387**, 56 (1997)] have reported catching a powerful flare in one of the sources with a peak luminosity of  $\sim 10^{34}$  to  $10^{36}\ \text{erg s}^{-1}$ . Thus, extending the spectrum to unobserved energies and accounting for very large flares yield a typical time-averaged  $L_x^{\text{tot}}$  for embedded protostars  $\geq 10^{31}\ \text{erg s}^{-1}$ .
13. R. Pallavicini, S. Serio, G. S. Vaiana, *Astrophys. J.* **216**, 108 (1977).
14. S. W. Kahler, *Annu. Rev. Astron. Astrophys.* **30**, 113 (1992).
15. J. T. Gosling, *J. Geophys. Res.* **98**, 4529 (1993).
16. D. V. Reames, *Rev. Geophys.* **33** (suppl.), 585 (1995).
17. H. Chen, P. C. Myers, E. F. Ladd, D. O. S. Wood, *Astrophys. J.* **445**, 377 (1995).
18. S. V. Beckwith and A. I. Sargent, in (7), pp. 521–542; N. Ohashi, M. Hayashi, R. Kawabe, M. Ishiguro, *Astrophys. J.* **466**, 317 (1996).
19. P. Ghosh and F. K. Lamb, *Astrophys. J.* **232**, 259 (1979); M. Livio and J. E. Pringle, *Mon. Not. R. Astron. Soc.* **259**, 23 (1992).
20. F. Shu *et al.*, *Astrophys. J.* **429**, 781 (1994); F. Shu, J. Najita, S. Ruden, S. Lizano, *ibid.*, p. 797; J. Najita and F. Shu, *ibid.*, p. 808; F. Shu, J. Najita, E. Ostriker, H. Shang, *ibid.* **455**, L155 (1995).
21. F. H. Shu, H. Shang, T. Lee, *Science* **271**, 1545 (1996).
22. E. D. Feigelson, *Icarus* **51**, 155 (1982).
23. E. N. Parker, *Astrophys. J.* **128**, 664 (1958).
24. E. Ostriker and F. Shu, *ibid.* **447**, 813 (1995).
25. D. Biskamp, *Nonlinear Magnetohydrodynamics* (Cambridge Univ. Press, Cambridge, 1993).
26. G. Herbig, *Adv. Astron. Astrophys.* **1**, 47 (1962); G. Herbig and N. K. Rao, *Astrophys. J.* **174**, 401 (1972); M. Cohen and L. V. Kuhi, *Astrophys. J. Suppl.* **41**, 743 (1979).
27. C. M. Johns and G. Basri, *Astrophys. J.* **449**, 341 (1995); C. M. Johns-Krull and A. P. Hatzes, *ibid.*, in press.
28. C. M. Johns and G. Basri, *ibid.* **474**, 433 (1997).
29. J. Eisloffel, R. Mundt, K.-H. Böhm, *Astron. J.* **108**, 1042 (1994); R. Gredel and B. Reipurth, *Astrophys. J.* **407**, L29 (1993).
30. A. C. Raga, *Rev. Mex. Astron. Astrofis. Ser. Conf.* **1**, 103 (1995).
31. G. H. Herbig, *Astrophys. J.* **217**, 693 (1977); L. Hartmann, S. Kenyon, P. Hartigan, in *Protostars and Planets III*, E. H. Levy and J. I. Lunine, Eds. (Univ. of Arizona Press, Tucson, AZ, 1993), pp. 497–518; K. R. Bell and D. N. C. Lin, *Astrophys. J.* **427**, 987 (1994).
32. F. L. Whipple, in *From Plasma to Planet*, A. E. Elvius, Ed. (Wiley, New York, 1972), pp. 211–232; S. J. Weidenschilling, *Mon. Not. R. Astron. Soc.* **180**, 57 (1977); J. N. Cuzzi, A. R. Dobrovolskis, J. M. Champney, *ibid.* **106**, 102 (1993); A. G. W. Cameron, *Meteoritics* **30**, 133 (1995); J. A. Wood, in *Chondrules and the Protoplanetary Disk*, R. H. Hewins, R. H. Jones, E. R. D. Scott, Eds. (Cambridge Univ. Press, New York, 1996), pp. 55–69.
33. M. R. Meyer, N. Calvet, L. A. Hillenbrand, *Astron. J.* **114**, 288 (1997).
34. Y. Yu, R. H. Hewins, B. Zanda, in *Chondrules and the Protoplanetary Disk*, R. H. Hewins, R. H. Jones, R. D. Scott, Eds. (Cambridge Univ. Press, Cambridge, 1996), pp. 213–220.
35. R. H. Hewins, in *Meteorites and the Early Solar System*, J. F. Kerridge and M. S. Matthews, Eds. (Univ. of Arizona Press, Tucson, AZ, 1988), pp. 660–679.
36. A. G. W. Cameron, *Annu. Rev. Astron. Astrophys.* **26**, 441 (1988); S. S. Russell, G. Srinivasan, G. R. Huss, G. J. Wasserburg, G. J. MacPherson, *Science* **273**, 757 (1996).
37. J. W. Larimer and J. T. Wasson, in *Meteorites and the Early Solar System*, J. F. Kerridge and M. S. Matthews, Eds. (Univ. of Arizona Press, Tucson, AZ, 1988), pp. 394–435.
38. J. A. Linker and Z. Mikić, *Astrophys. J.* **438**, L45 (1995); Z. Mikić, *ibid.* **430**, 898 (1994).
39. M. R. Hayashi, K. Shibata, R. Matsumoto, *ibid.* **468**, L37 (1996); A. P. Goodson, R. M. Winglee, K.-H. Böhm, in preparation; K. Miller and J. Stone, *Astrophys. J.*, in press.
40. W. Fowler, J. Greenstein, F. Hoyle, *Geophys. J. R. Astron. Soc.* **6**, 148 (1962).
41. D. D. Clayton and L. Jin, *Astrophys. J.* **451**, L87 (1995).
42. T. Lee, F. H. Shu, H. Shang, A. E. Glassgold, in preparation.
43. Supported by a NASA grant from the Origins of Solar Systems Program (to E.H.S., H.S., and A.E.G.) and by Republic of China National Science Council grants 85-2112-M001-024 and 86-2112-M001-033 (to T.L.). We thank E. Feigelson, L. Hartmann, R. Lin, D. Longcope, J. Luhmann, T. Montmerle, and E. Ostriker for illuminating discussions.

15 April 1997; accepted 24 July 1997